LA-UR-16-28981
Approved for public release; distribution is unlimited.

Title: Parameterization of a Cookoff Model for LX-07

Author(s): Aviles-Ramos, Cuauhtemoc

Intended for: Report

Issued: 2016-11-22

Parameterization of a Cookoff Model for LX-07

Cuauhtemoc Aviles–Ramos
Los Alamos National Laboratory
Advanced Engineering Analysis, W-13
Los Alamos, New Mexico 87545

ABSTRACT

A thermal decomposition model for PBX 9501 (95% HMX, 2.5% Estane® binder, 2.5% BDNPA/F nitro-plasticizer) was implemented by Dickson, et. al [1]. The objective in this study is to estimate parameters associated with this kinetics model so it can be applied to carry out thermal ignition predictions for LX-07 (90% HMX, 10% Viton binder). LX-07 thermal ignition experiments have been carried out using the "Sandia Instrumented Thermal Ignition Apparatus", SITI [2]. The SITI design consists of solid cylinders (1" diameter × 1" height) of high explosive (HE) confined by a cylindrical aluminum case. An electric heater is wrapped around the outer surface of the case. This heater produces a temperature heating ramp on the outer surface of the case. Internal thermocouples measure the HE temperature rise from the center to locations close to the HE-aluminum interface. The energetic material is heated until thermal ignition occurs. A two–dimensional axisymmetric heat conduction finite element model is used to simulate these experiments. The HE thermal decomposition kinetics is coupled to a heat conduction model trough the definition of an energy source term. The parameters used to define the HE thermal decomposition model are optimized to obtain a good agreement with the experimental time to thermal ignition and temperatures. Also, heat capacity and thermal conductivity of the LX-07 mixture were estimated using temperatures measured at the center of the HE before the solid to solid HMX phase transition occurred.

HMX THERMAL DECOMPOSITION MODEL

Dickson, et. al [1] implemented an irreversible PBX 9501 thermal decomposition model that considers 4 steps in the thermal decomposition reaction mechanism

$$
\begin{aligned}
&1)\ \mathrm{HMX}\ (\beta) \rightarrow \mathrm{HMX}\ (\delta) \\
&\quad (\text{first order endothermic}) \\
&2)\ \mathrm{HMX}\ (\beta) + \mathrm{HMX}\ (\delta) \rightarrow \mathrm{HMX}\ (\delta) \\
&\quad (\text{bimolecular endothermic}) \\
&3)\ \mathrm{HMX}\ (\delta) \rightarrow \textit{products} \\
&\quad (1^{st}\ \text{order endothermic}) \\
&4)\ \mathrm{HMX}\ (\delta) + \textit{products}(\mathrm{gas}) \rightarrow \textit{products}(\mathrm{gas}) \\
&\quad (\text{bimolecular exothermic})
\end{aligned}
\qquad (1)
$$

The associated rate equations are given by [1]

$$r_1 = M_a \frac{kT}{h} \exp\left(\frac{T\Delta S_1 - E_1 - P\Delta V}{RT}\right) \tag{2}$$

$$r_2 = M_a M_b \frac{kT}{h} \exp\left(\frac{T\Delta S_2 - E_2 - P\Delta V}{RT}\right) \tag{3}$$

$$r_3 = M_b Z_3 \exp\left(\frac{-E_3}{RT}\right) \tag{4}$$

$$r_4 = M_b M_c Z_4 \exp\left(\frac{-E_4}{RT}\right) \tag{5}$$

where M_a, M_b, and M_c are the mass fractions of β–HMX, δ–HMX, and gas products respectively. The quantities $\Delta S_1, \Delta S_2, E_1, E_2, E_3, E_4, Z_3, Z_4,$ and ΔV are expressed per mole and are given in Table 1. Also, *k* represents Boltzmann's constant and *h* is Planck's constant.

Table 1. Ignition kinetics parameters for PBX 9501 mechanism (1) given in reference [1].

Step #	*Z*, (1/s)	ΔS (J mol^{-1} K^{-1})	*E* (J mol^{-1})	ΔV (m^3 mol^{-1})	ΔH (kJ kg^{-1})
1		136	2.05×10^5	0	– 25
2		630	4.13×10^5	0	– 25
3	3.16×10^{16}		2.00×10^5		– 1200
4	8.0×10^{15}		1.75×10^5		3200

The system that represents the thermal decomposition model is obtained from the principle of conservation of mass

$$\frac{\partial M_a}{\partial t} = -r_1 - r_2 \tag{6}$$

$$\frac{\partial M_b}{\partial t} = r_1 + r_2 - r_3 - r_4 \tag{7}$$

$$\frac{\partial M_c}{\partial t} = r_3 + r_4 \tag{8}$$

The energy source term is defined as

$$Q = \rho \sum_{j=1}^{4} \Delta H_j \; r_j \tag{9}$$

where ρ is the density of the HE mixture. The volumetric heat generation term, Eq. (9), is coupled with the heat conduction equation in the HE

$$\frac{1}{r}\frac{\partial}{\partial r}\left(k(T)\, r\frac{\partial T}{\partial r}\right)+\frac{\partial}{\partial z}\left(k(T)\frac{\partial T}{\partial z}\right)+Q=\rho C_p(T)\frac{\partial T}{\partial t} \tag{10}$$

where $k(T)$ and $c_p(T)$ are the HE mixture thermal conductivity and heat capacity defined as weighted averages of the mass fractions as

$$k(T)=M_a(a_1+b_1T)+M_b(a_2+b_2T)+M_c(a_3+b_3T) \tag{11}$$

$$c_p(T)=M_a(c_1+d_1T)+M_b(c_2+d_2T)+M_c(c_3+d_3T) \tag{12}$$

Notice from Eqs. (11) and (12) that the thermal properties of β–HMX and δ–HMX are linear functions of temperature. The parameters for PBX 9501 in Eqs. (11) and (12) [1] are given in Table 2

Table 2. Parameters for PBX 9501 thermal properties in Eqs. (11) and (12) [1].

i	a_i (J m^{-1}K^{-1}s^{-1})	b_i (J m^{-1}K^{-2}s^{-1})	c_i (J kg^{-1}K^{-1})	d_i (J kg^{-1}K^{-2})
1	1.42	-2.08×10^{-3}	236	2.7
2	0.53	-5.40×10^{-4}	236	2.7
3	2.0	0.0	222	2.45

SIMULATION OF LX-07 THERMAL DECOMPOSITION EXPERIMENTS

The finite element heat transfer code Aria [3] is used to simulate the LX-07 SITI [2] experiments. Figure 1 shows a sketch of a SITI apparatus. The thermal decomposition model for PBX 9501 described in the previous section is used first to simulate the SITI experiments to evaluate the differences between this model (using the PBX 9501 parameters) and the experimental response of LX-07. A summary of the SITI LX-07 experiments is given in Table 3

Table 3. Summary of LX-07 experiments

Run #	Boundary Temperature, °C	Time to ignition, seconds
301	199	18037
247	201	16472
300	201	16440
299	204	10267
297	208	5781
303	212	4608

The mesh used for these simulations is shown in Fig 2. An axisymmetric two-dimensional model that contains linear quadrilateral elements was used. The geometry features that influence the heat transfer in the specimen were considered.

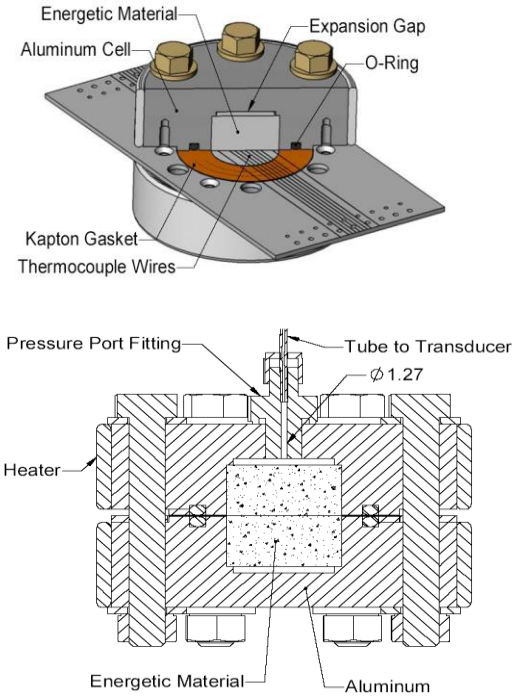

Figure 1. Sandia Instrumented Thermal Ignition apparatus [2].

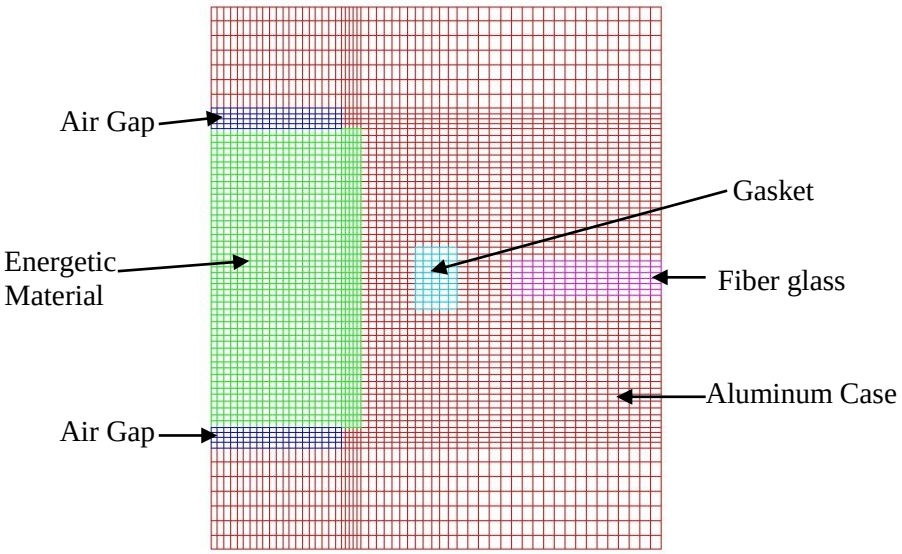

Figure 2. Two-dimensional axisymmetric mesh for SITI apparatus.

The SITI experiments [2] provide information about the boundary conditions on the top, bottom, and lateral surfaces of the aluminum case in the form of thermocouple measurements. These measurements were incorporated into the finite element model. Figure 3 shows an internal temperature measurement and the boundary condition thermocouples

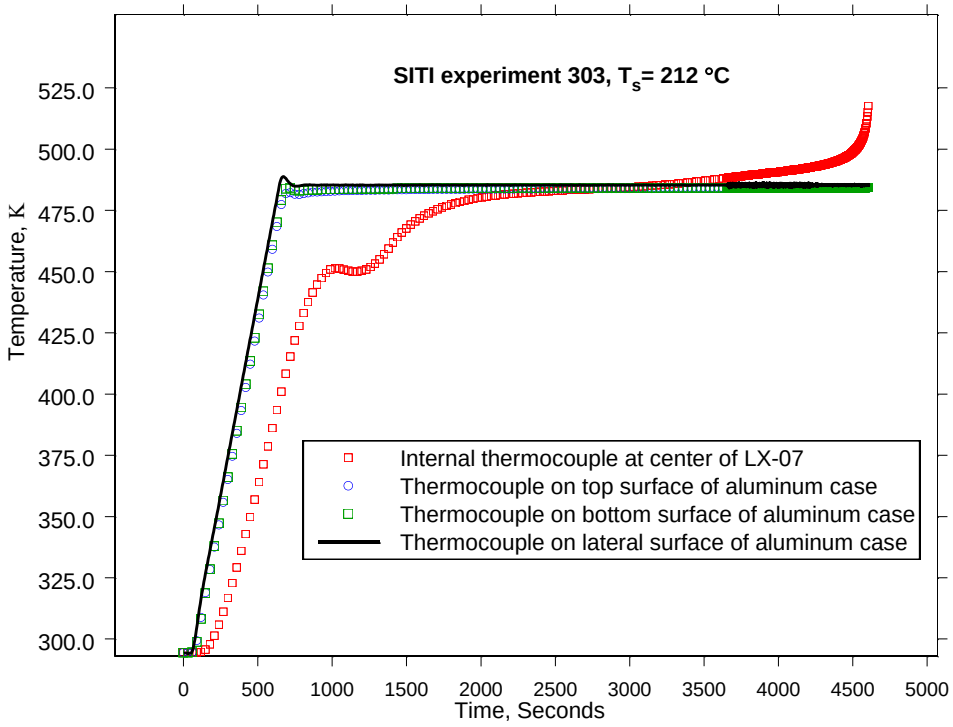

Figure 3. Temperature measurements for LX-07 SITI experiment # 303.

Measurements like the ones shown in Fig. 3 are used to carry out simulations and comparisons with the finite element model response in the mid-plane of the HE. Table 4 shows the thermal ignition prediction errors given by the model represented by Eqs. (1)–(10) and using the PBX 9501 kinetic and thermal parameters shown in Tables 1 and 2

Table 4. Predicted thermal ignition times given by Eqs. (1)–(10) and using kinetic and thermal parameters shown in Tables 1 and 2.

SITI Run #	Boundary Temperature, °C	Experimental Time to ignition, seconds	Predicted Time to ignition, Seconds	Error, %
301	199	18037	6654	63
247	201	16472	5380	67
300	201	16440	5365	67
299	204	10267	4149	60
297	208	5781	3090	46
303	212	4608	2467	46

Table 4 shows that the PBX 9501 model under predicts 6 thermal ignition times for LX-07 with errors larger than 45%. This is to be expected because the PBX 9501 binder decomposes exothermically while the LX-07 binder (Viton) undergoes an endothermic decomposition. Figures 4 and 5 show comparisons between the PBX 9501 model response and internal temperature measurements in the LX-07 explosive.

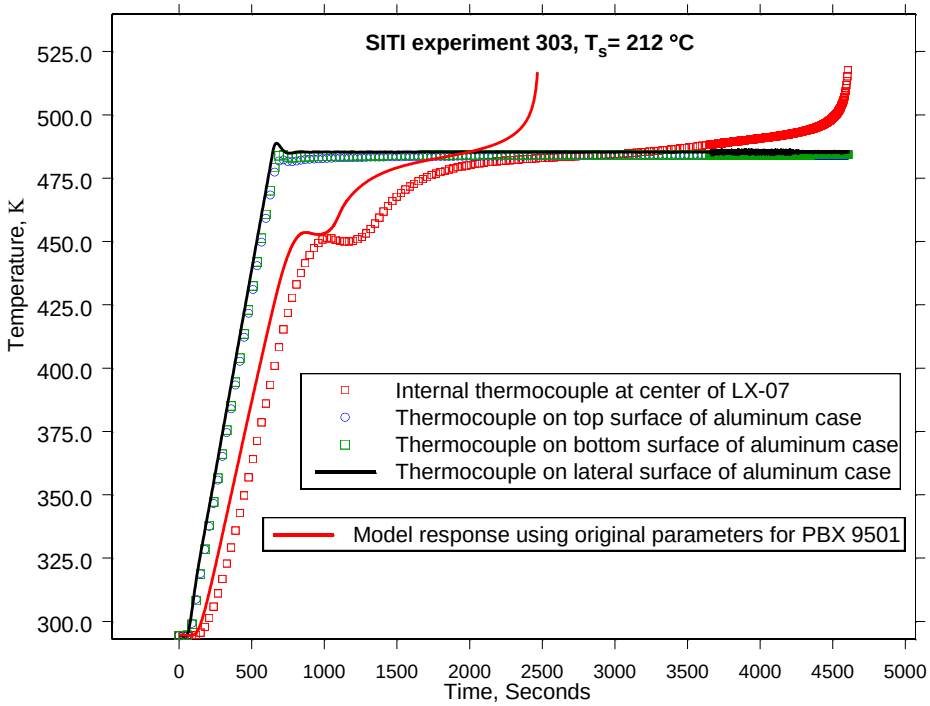

Figure 4. Comparison of PBX 9501 model response, Eqs. (1)–(10), with LX-07 experiment # 303.

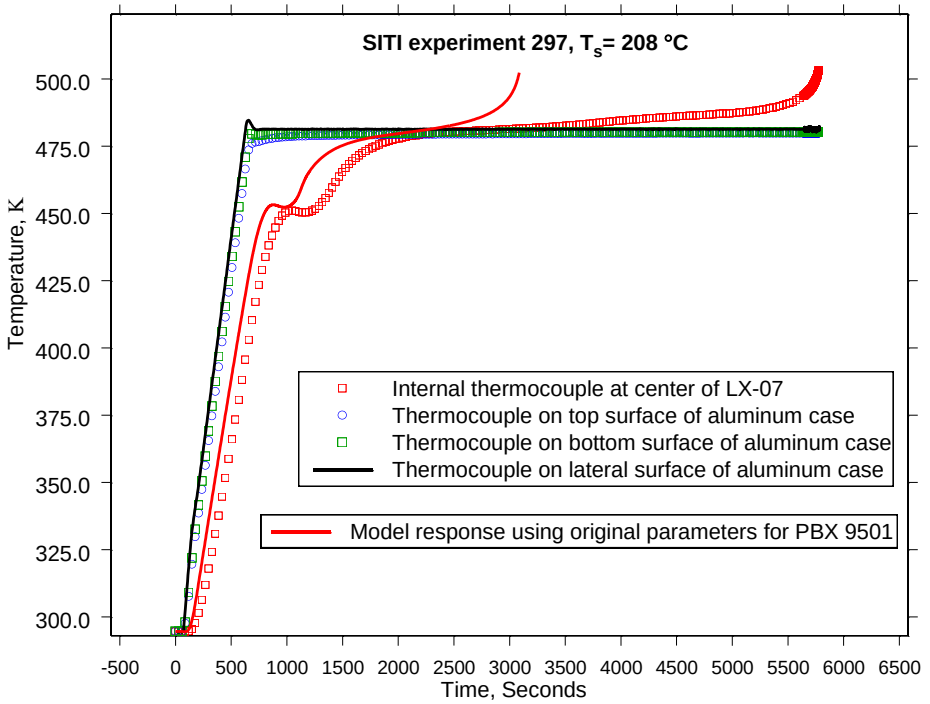

Figure 5. Comparison of PBX 9501 model response, Eqs. (1)–(10), with LX-07 experiment # 297.

Figures 4 and 5 show that there are significant differences between the temperature traces produced by the PBX 9501 thermal decomposition model and the measured temperatures inside the LX-07 explosive. These differences become more evident prior to the HMX phase change from β to δ phase. This is an endothermic phase change which is noticeable by a temperature decrease (and a subsequent increase) of the LX-07 internal thermocouple traces around 450 K. Differences between the predicted and measured traces shown in Figs. 4 and 5 also show that there is a need to estimate the thermal properties of the LX-07 mixture. This is to be expected because Viton has different thermal properties than the Estane and BDNPA/F nitro-plasticizer.

The differences shown by Table 3 and Figs. 4 and 5 prompted the optimization of the kinetic and thermal parameters that define the model given by Eqs. (1)–(10). This optimization process starts with a sensitivity analysis to identify the parameters that have a stronger influence on the time to thermal ignition. It is expected that by optimizing the most influential parameters, the error in the prediction of thermal ignition time can be decreased in the global sense. The model given by Eqs. (1)–(10) was originally developed for PBX 9501. An attempt to optimize the parameters associated with this model is made here so it can be used to carry out predictions involving the LX-07 explosive.

ESTIMATION OF THERMAL AND KINETIC PARAMETERS FOR THE LX-07 THERMAL DECOMPOSITION MODEL

To distinguish the thermal parameters between PBX 9501 and LX-07, the thermal properties for LX-07 are defined as

$$k^*(T) = M_a k_\beta + M_b k_\delta + M_c k_g \tag{13}$$

$$C_p^*(T) = M_a C_{p\beta} + M_b C_{p\delta} + M_c C_{pg} \tag{14}$$

where $k_\beta, k_\delta,$ and k_g are the thermal conductivities of LX-07(β), LX-07(δ), and decomposition gases respectively. Also, $C_{p\beta}, C_{p\delta},$ and C_{pg} are the heat capacities of LX-07(β), LX-07(δ), and decomposition gases respectively. The decomposition gases thermal properties were left unchanged and only the thermal properties of LX-07(β) and LX-07(δ) were estimated. The thermal conductivities and heat capacities of LX-07(β) and LX-07(δ) were assumed to be linear functions of temperature. Table 5 shows the estimated parameters

$$k_\beta = a_1^* + b_1^* T, \qquad k_\delta = a_2^* + b_2^* T \tag{15}$$

$$C_{p\beta} = c_1^* + d_1^* T \tag{16}$$

$$C_{p\delta} = \begin{cases} c_2^* + d_2^* T & \text{for } T \le 463\,\text{K} \\ c_3^* + d_3^* T & \text{for } T > 463\,\text{K} \end{cases} \tag{17}$$

Table 5. Estimated parameters for LX-07 thermal properties, Eqs. (15)–(17).

i	a_i^* (J m^{-1}K^{-1}s^{-1})	b_i^* (J m^{-1}K^{-2}s^{-1})	c_i^* (J kg^{-1}K^{-1})	d_i^* (J kg^{-1}K^{-2})
1	0.7161	-8.4521×10^{-4}	434.3721	2.5718
2	0.4770	-4.8600×10^{-4}	712.3818	4.2179
3	–	–	395.2656	2.3403

The activation energy E_4 associated with step 4) of the mechanism, HMX (δ) + *products* → *products*, has a significant influence on the time to thermal ignition. This becomes evident by looking at the four terms that define the volumetric heat generation source in numerical form

$$Q/\rho = -6.66146\times10^{18} M_a \exp\left(\frac{-2.214\times10^5}{RT}\right) - 4.205\times10^{44} M_a M_b \exp\left(\frac{-4.413\times10^5}{RT}\right)$$
$$-3.79\times10^{18} M_b \exp\left(\frac{-2.0\times10^5}{RT}\right) + 2.56\times10^{19} M_b M_c \exp\left(\frac{-1.74\times10^5}{RT}\right) \qquad (18)$$

Since the HMX β to δ phase change reactions 1) and 2) are irreversible, the HMX β phase mass fraction M_a tends to zero at the end of the phase transition. This has the effect of making the sum of the first two terms in Eq. (18) smaller than the fourth term after the phase transition. Also, at times when the thermocouple readings at the center of the LX-07 in Figs. 4 and 5 become closer or larger than the boundary temperatures, the fourth term in Eq. (18) is larger than the rest of the terms making the quantity Q/ρ greater than zero. This effect causes the last term in Eq. (18) to be the dominant term for the production of energy at this stage in the decomposition process. This is why the activation energy E_4 has a significant influence on the time to thermal ignition. This behavior was corroborated making parametric studies that included variations of the activation energy E_4 while keeping the rest of the thermal and kinetic parameters constant. These parametric studies revealed that there is an optimum activation energy E_4 that predicts the experimental time to thermal ignition for each one of the experiments shown in Table 4. These results are shown in Table 6

Table 6. Predicted thermal ignition times given by Eqs. (1)–(10) using the parameters Shown in Table 1 with the exception of ΔH_3 which was set equal to -3000 J/g. The thermal properties estimated in Table 5 were used for these finite element predictions.

SITI Run #	Boundary Temperature, °C	E_4, J/mol	Experimental Time to ignition, seconds	Predicted Time to ignition, seconds	Error, %
301	199	1.79000×10^5	18037	18029	-0.04
247	201	1.79351×10^5	16472	16470	0.01
300	201	1.79448×10^5	16440	16442	-0.01
299	204	1.79000×10^5	10267	10269	-0.02
297	208	1.77958×10^5	5781	5780	-0.02
303	212	1.78362×10^5	4608	4609	0.02

Comparisons of the finite element response at the center of the LX-07 with the SITI temperature readings are shown in Figs. 6 and 7. The value of ΔH_3 was adjusted to get a better agreement with the experiments after the phase change. The agreement between the model and the experiments in Figs. 6 and 7 can be considered to be reasonable taking into account the degree of simplification of the kinetics model. A parametric study in the range of the activation energies

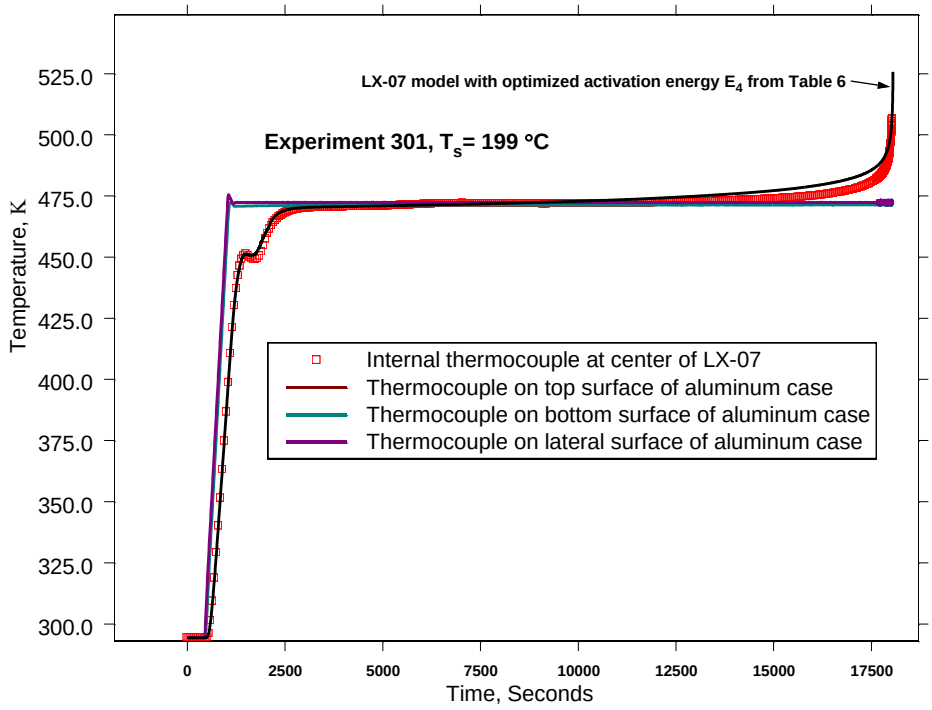

Figure 6. Comparison of the finite element response with the measured temperature at the center of LX-07 explosive for SITI experiment # 301 Prediction shown in first row of Table 6.

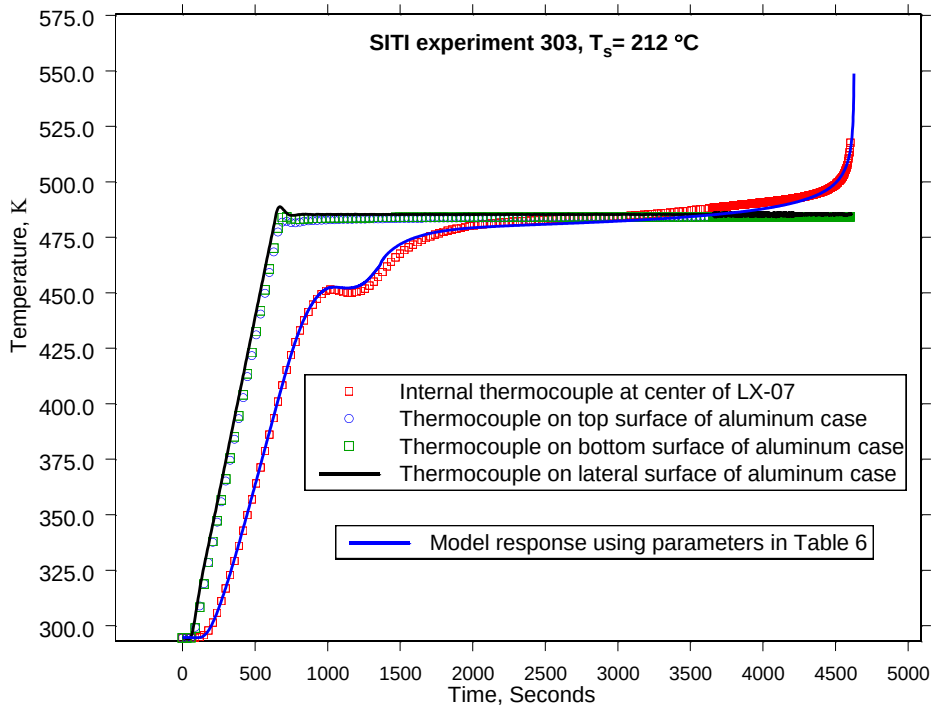

Figure 7. Comparison of the finite element response with the measured temperature at the center of LX-07 explosive for SITI experiment # 301 Prediction shown in sixth row of Table 6.

shown in Table 6 was carried out to see if a constant (or average) value of the activation energies produces a set of time to ignition errors with magnitudes smaller than 20%. Figure 8 shows the results of this parametric study.

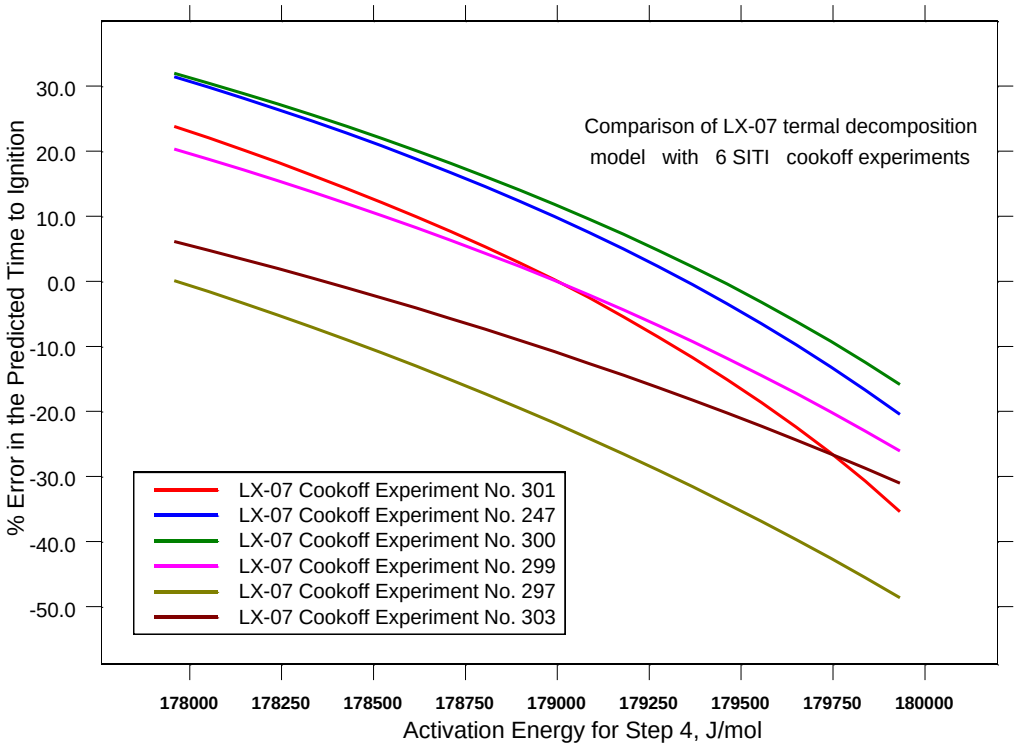

Figure 8. Parametric study carried out with 6 SITI [2] experiments for the the range of E_4 values shown in Table 6. Graph was generated by 132 simulations.

Figure 8 shows the percentage error in the predicted time to thermal ignition as a function of the activation energy of the fourth reaction step in (1). The parametric study shown in Fig. 8 was carried out automatically using a FORTRAN program coupled with the LX-07 finite element model. Note from Fig. 8 that a constant value of E_4 doesn't produce a set of time to ignition errors with magnitudes smaller than 20% for all the experiments. Also, note from Table 6 that the activation energy E_4 drops from an average value of 1.793×10^5 J/mol (for slow cook-off SITI experiments # 301, 247, 300, and 299) to an average value of 1.782×10^5 J/mol (for fast cook-off experiments # 297 and 303). The magnitude of this drop is about 1100 J/mol which is needed by the model to capture thermal ignition correctly for the fast cook-off cases in Table 6. This is an indication that the activation energy E_4 is an effective activation energy that is a function of temperature. Reference [5] discusses physical processes associated with the variation of the effective activation energy with temperature in liquids and solids. Reaction steps 1) through 4) don't consider the effects of the binder (Viton) decomposition. The omission of reaction steps associated with the decomposition of Viton might be causing the experimental activation energy estimated in Table 5 to be a function of temperature. As pointed out in the conclusions of reference [6]: "The phenomenon of variable activation energy is the everyday reality of the condensed phase processes that tend to involve multiple steps having differing activation

energies. By its meaning variable activation energy is an effective parameter that represents an interplay of individual steps." The variable activation energy was estimated as a quartic polynomial in temperature

$$r_4 = \begin{cases} M_b M_c\, Z_4 \exp\left(\dfrac{-E_{4,1}}{RT}\right) \text{ for } T \le T_1 \\ M_b M_c\, Z_4 \exp\left(\dfrac{-\sum_{j=0}^{4} p_j T^j}{RT}\right) \text{ for } T_1 < T < T_2 \\ M_b M_c\, Z_4 \exp\left(\dfrac{-E_{4,2}}{RT}\right) \text{ for } T \ge T_2 \end{cases} \tag{19}$$

where $E_{4,1} = E_{4,2} = 1.78362\times10^5$ J/mol, T_1=472.15 K, T_2=485.15 K, and the polynomial coefficients are given in Table 7. The predicted thermal ignition times using the FE model that includes Eqs. (1)–(4), (19), and (6)–(10) are given in Table 8. Table 8 shows errors with magnitudes smaller than 5.8 %. A comparison of Tables 4 and 8 shows that this parameterization reduced the average time to ignition error from 58% to 4%. This model also predicts the location of ignition. Figures 8 and 9 show comparisons of two simulations shown in Table 8 with experiments # 299 and 303 at the center of the LX-07 cylinders.

Table 7. Estimated polynomial coefficients defined in Eq. (19)

p_0, J/mol	p_1, J/mol K	p_2, J/mol K^2	p_3, J/mol K^3	p_4, J/mol K^4
-3.03462×10^8	2.51261×10^8	780061.	1076.23	- 0.556753

Table 8. Predicted thermal ignition times given by Eqs. (1)–(4), (19), and (6)–(10) using the parameters shown in Table 1 with the exception of ΔH_3 which is set equal to -3000 J/g. The thermal properties for LX-07 shown in Table 5 were used for these finite element predictions.

SITI Run #	Boundary Temperature, °C	Experimental Time to ignition, seconds	Predicted Time to ignition, seconds	Error, %
301	199	18037	18990	-5.3
247	201	16472	15996	2.9
300	201	16440	15488	5.8
299	204	10267	9868	3.9
297	208	5781	6100	-5.4
303	212	4608	4532	1.6

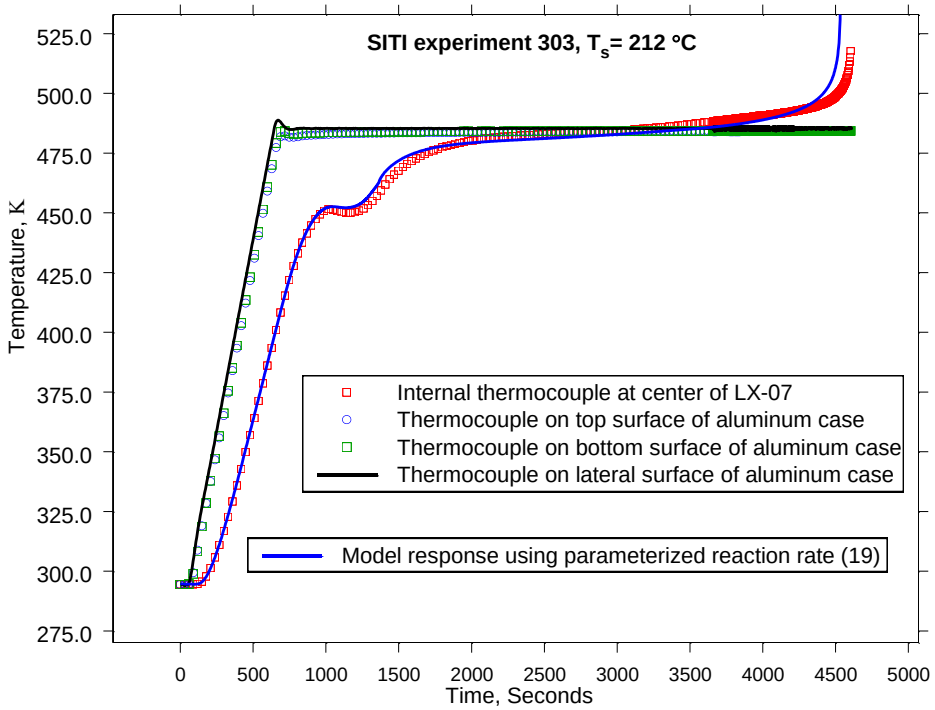

Figure 8. Comparison of experiment 303 with the model described in Table 7.

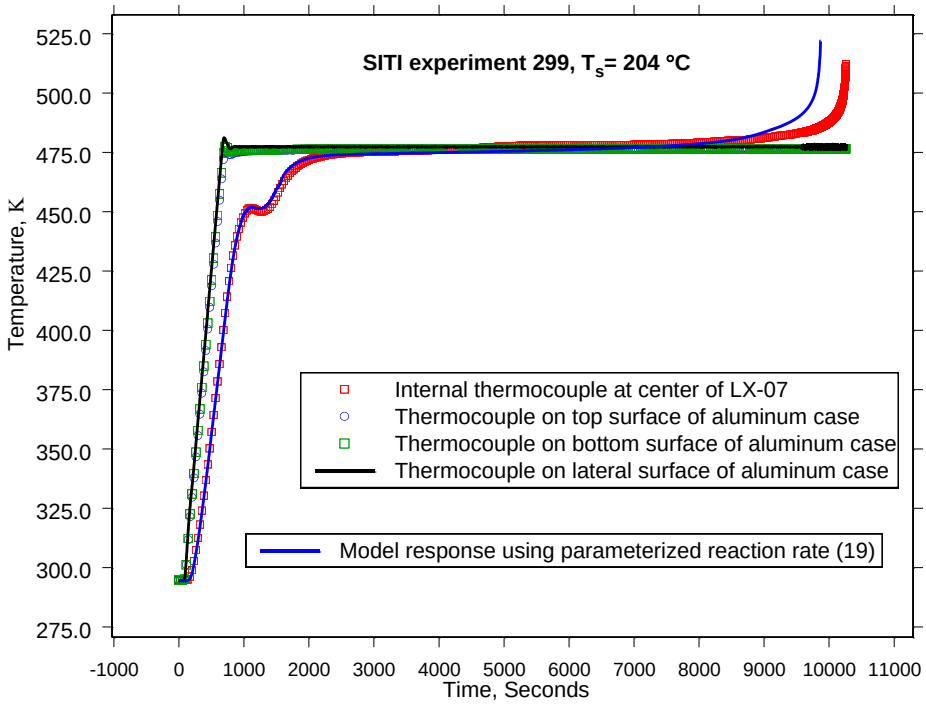

Figure 9. Comparison of experiment 299 with the model described in Table 7.

COMMENTS

The LX-07 thermal properties shown in Table 5 were estimated using internal thermocouple readings from the SITI experiment # 173. Thermocouple readings in a time interval where reaction steps 3) and 4) in Eq. (1) are practically inactive were used for these estimations. This corresponds to an interval from time equal zero to a time after the HMX phase change from β to δ has taken place. A FORTRAN program was written to couple the finite element model with a parameter estimation algorithm. An algorithm without derivatives due to Powell [4] was used for this case. Ten parameters were estimated to define the thermal conductivity and heat capacity of LX-07 as linear functions of temperature shown in Table 5. Also, ten parameters associated with the kinetics model were estimated from the SITI experiments shown in Table 8. These kinetics parameters include ΔH_3, five polynomial coefficients (Table 7), $E_{4,1}$, $E_{4,2}$, T_1, and T_2 which were used to define the rate of reaction, r_4, in Eq. (19). This model predicts the time to thermal ignition with an error magnitude less or equal than 5.8% (Table 8).

REFERENCES

[1] P. M. Dickson, B. W. Assay, B. F. Henson, C. S. Fugard, J. Wong, "Measurement of Phase Change and Thermal Decomposition Kinetics During Cookoff of PBX 9501," CP505, *Shock Compression of Condensed Matter*, edited by M. D. Furnish, L. C. Chhabildas, and R. S. Hixson © 2000 American Institute of Physics, l-56396-923-8.

[2] M.J. Kaneshige, A. M. Renlund, R. G. Schmitt, and W. W. Erickson, "Improvements in Cook–off Models Using Real–Time in Situ Measurement of Temperature and Pressure," SAND2003–4419C, 2003 JANNAF Propulsion Systems Hazards Subcommittee Meeting, Colorado Springs, CO (1–5 Dec 2003).

[3] Notz, P. K., Subia, S. R., Hopkins, M. M, Moffat, H. K., Noble, D. R., "Aria 1.5: User Manual," Sandia Report SAND2007-2734, Sandia National Laboratories, P. O. Box 5800, Albuquerque, NM 87185, 2007.

[4] Press, W. H., Teukolsky, S. A., Vetterling, W. T., and Flannery, B. P., "*Numerical Recipes in FORTRAN. The Art of Scientific Computing*," 2nd ed. Published by the Press Syndicate of the University of Cambridge, The Pitt Building, Trumpington Street, Cambridge CB2 1RP, Copyright © Cambridge University Press, 1986, 1992.

[5] Vyazovkin, S., "On the phenomenon of variable activation energy for condensed phase reactions," *New J. Chem.*, 2000, **24,** 913–917.

[6] Vyazovkin, S., "A time to search: finding the meaning of variable activation energy," *Phys. Chem. Chem. Phys.*, 2016, **18,** 18643-18656.